UNIVERSITY OF BIRMINGHAM
University of Birmingham Research at Birmingham

Iridium nanoparticles for multichannel luminescence lifetime imaging, mapping localization in live cancer cells

King, Siobhan M; Claire, Sunil; Teixeira, Rodolfo I; Dosumu, Abiola N; Carrod, Andrew J; Dehghani, Hamid; Hannon, Michael J; Ward, Andrew D; Bicknell, Roy; Botchway, Stanley W; Hodges, Nikolas J; Pikramenou, Zoe

DOI:
10.1021/jacs.8b05105

License:
Other (please specify with Rights Statement)

Document Version
Publisher's PDF, also known as Version of record

Citation for published version (Harvard):
King, SM, Claire, S, Teixeira, RI, Dosumu, AN, Carrod, AJ, Dehghani, H, Hannon, MJ, Ward, AD, Bicknell, R, Botchway, SW, Hodges, NJ & Pikramenou, Z 2018, 'Iridium nanoparticles for multichannel luminescence lifetime imaging, mapping localization in live cancer cells', *Journal of the American Chemical Society*, vol. 140, no. 32, pp. 10242-10249. https://doi.org/10.1021/jacs.8b05105

Link to publication on Research at Birmingham portal

Publisher Rights Statement:
This is an open access article published under an ACS AuthorChoice License, which permits copying and redistribution of the article or any adaptations for non-commercial purposes.

General rights
Unless a licence is specified above, all rights (including copyright and moral rights) in this document are retained by the authors and/or the copyright holders. The express permission of the copyright holder must be obtained for any use of this material other than for purposes permitted by law.

•Users may freely distribute the URL that is used to identify this publication.
•Users may download and/or print one copy of the publication from the University of Birmingham research portal for the purpose of private study or non-commercial research.
•User may use extracts from the document in line with the concept of 'fair dealing' under the Copyright, Designs and Patents Act 1988 (?)
•Users may not further distribute the material nor use it for the purposes of commercial gain.

Where a licence is displayed above, please note the terms and conditions of the licence govern your use of this document.

When citing, please reference the published version.

Take down policy
While the University of Birmingham exercises care and attention in making items available there are rare occasions when an item has been uploaded in error or has been deemed to be commercially or otherwise sensitive.

If you believe that this is the case for this document, please contact UBIRA@lists.bham.ac.uk providing details and we will remove access to the work immediately and investigate.

Download date: 05. May. 2023

This is an open access article published under an ACS AuthorChoice License, which permits copying and redistribution of the article or any adaptations for non-commercial purposes.

JACS
JOURNAL OF THE AMERICAN CHEMICAL SOCIETY
Article
Cite This: J. Am. Chem. Soc. 2018, 140, 10242−10249
pubs.acs.org/JACS

Iridium Nanoparticles for Multichannel Luminescence Lifetime Imaging, Mapping Localization in Live Cancer Cells

Siobhan M. King,[†,‡] Sunil Claire,[‡] Rodolfo I. Teixeira,[‡] Abiola N. Dosumu,[§] Andrew J. Carrod,[‡] Hamid Dehghani,[∥] Michael J. Hannon,[†,‡] Andrew D. Ward,[#] Roy Bicknell,[⊥] Stanley W. Botchway,[#] Nikolas J. Hodges,[§] and Zoe Pikramenou[‡,*]

[†]The Centre of Physical Sciences of Imaging in Biomedical Sciences, [‡]School of Chemistry, [§]School of Biosciences, [∥]School of Computer Science, and [⊥]Institute of Cardiovascular Sciences, University of Birmingham, Edgbaston B15 2TT, United Kingdom
[#]Central Laser Facility, Rutherford Appleton Laboratory, Research Complex Harwell, STFC, Didcot OX11 0QT, United Kingdom

Supporting Information

ABSTRACT: The development of long-lived luminescent nanoparticles for lifetime imaging is of wide interest as luminescence lifetime is environmentally sensitive detection independent of probe concentration. We report novel iridium-coated gold nanoparticles as probes for multiphoton lifetime imaging with characteristic long luminescent lifetimes based on iridium luminescence in the range of hundreds of nanoseconds and a short signal on the scale of picoseconds based on gold allowing multichannel detection. The tailor-made IrC_6 complex forms stable, water-soluble gold nanoparticles (AuNPs) of 13, 25, and 100 nm, bearing 1400, 3200, and 22 000 IrC_6 complexes per AuNP, respectively. The sensitivity of the iridium signal on the environment of the cell is evidenced with an observed variation of lifetimes. Clusters of iridium nanoparticles show lifetimes from 450 to 590 ns while lifetimes of 660 and 740 ns are an average of different points in the cytoplasm and nucleus. Independent luminescence lifetime studies of the nanoparticles in different media and under aggregation conditions postulate that the unusual long lifetimes observed can be attributed to interaction with proteins rather than nanoparticle aggregation. Total internal reflection fluorescence microscopy (TIRF), confocal microscopy studies and 3D luminescence lifetime stacks confirm the presence of bright, nonaggregated nanoparticles inside the cell. Inductively coupled plasma mass spectrometry (ICPMS) analysis further supports the presence of the nanoparticles in cells. The iridium-coated nanoparticles provide new nanoprobes for lifetime detection with dual channel monitoring. The combination of the sensitivity of the iridium signal to the cell environment together with the nanoscaffold to guide delivery offer opportunities for iridium nanoparticles for targeting and tracking in in vivo models.

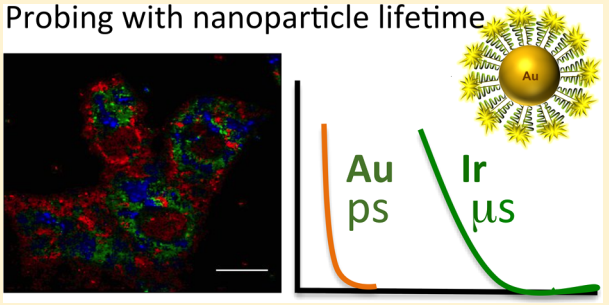

INTRODUCTION

Multiphoton imaging is fast becoming the most widely used optical microscopy for in vivo experiments with breakthroughs in medical diagnostics, specifically in quantification of angiogenesis and cancer metastasis, reaching to several millimeters in depth detection, thus providing invaluable information on tumor vasculature and tumor microenvironment.[1−3] Combining multiphoton excitation with lifetime imaging microscopy reveals a wealth of additional information, which is independent of the probe concentration but sensitive to local changes of the environment.[4,5] Nanoparticles in imaging applications have gained a lot of attention for providing high sensitivity, leading to improved spatial resolution while requiring lower concentrations compared to molecular probes and allowing versatile targeting vector attachment.[6,7] In multiphoton imaging, their applications have been restricted in the selection of the organic dye or the properties of the materials, which have short-lived luminescence signals.[8−12] There is a strong interest for the development of probes with long excited state lifetimes, which can be gated from short-lived signals associated with autofluorecence, expanding sensitivity in signal detection.[13] Iridium cyclometalated complexes are popular luminescent probes for biological imaging,[14,15] with a luminescent signal that can be tuned by modification of their ligand framework which also influences localization in cell organelles.[16,17] The power of detection by lifetime imaging of metal complexes[18] is demonstrated in iridium complexes in tumor imaging for cancer metastasis[19] and hypoxia.[20]

We have been interested in the development of nanosized probes based on gold scaffold and luminescent transition metal complexes in order to translate the attractive luminescent properties of the metal complexes to the nanosized probe.[21−23] The coating of transition metal allows covering of the gold surface with hundreds to thousands of metal complexes which

Received: May 17, 2018
Published: July 21, 2018

Downloaded via UNIV OF BIRMINGHAM on March 13, 2019 at 13:19:02 (UTC).
See https://pubs.acs.org/sharingguidelines for options on how to legitimately share published articles.

© 2018 American Chemical Society

DOI: 10.1021/jacs.8b05105
J. Am. Chem. Soc. 2018, 140, 10242−10249

give a strong characteristic luminescent signal. Gold nanoparticles have unique optical properties and can easily incorporate more than one type of imaging or targeting agent, which allows them to be used as multifunctional nanoplatforms for both imaging and cancer therapies.[24] The gold nanoparticle scaffold is ideal as a multimodal probe which can be detected by electron microscopy techniques as well as reflectance microscopy, which is highly advantageous for 100 nm gold nanoparticles to be detected as single, nonaggregated particles within the microscope diffraction limit.[25,26] Even though the characteristic surface plasmon resonance of the gold nanospheres has been used extensively as signal detection,[27] there is little investigation in monitoring gold nanoparticles by lifetime imaging.[28]

In this paper, we introduce iridium coated nanoparticles for multichannel lifetime imaging using multiphoton excitation. We have developed a novel nanoprobe based on a luminescent iridium complex with long legs for attachment to gold (Scheme 1). It was previously shown that the distance of the

Scheme 1. Schematic for Procedure of Coating AuNPs with Fluorinated Surfactant and IrC_6

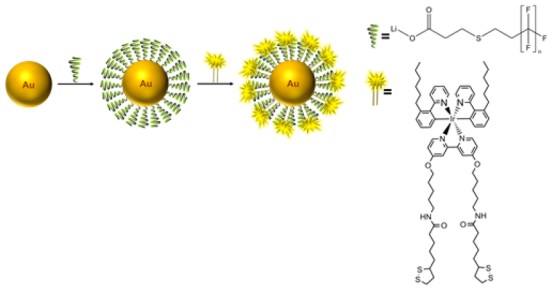

luminescent center from the gold nanoparticle enhances the lifetime properties of the ruthenium probes.[22] Incorporating the hexyl chain on the phenylpyridine was designed to increase hydrophobicity of the iridium complex and stabilization onto gold, increasing signal and therefore proposing better permeability across the cell membrane.[29,30] We illustrate in this paper detection of the characteristic long lifetime of the iridium complex and the short lifetime detected from the gold resonance signal by lifetime imaging microscopy. We have examined different sizes of gold nanoparticles (13, 25, and 100 nm) functionalized with the iridium probe and their uptake in live HeLa cells with lifetime imaging, optical and electron based techniques. The sizes were selected based on previous studies which show that the coated gold nanoparticles within the 10- 60 nm range show high uptake into cancer cells.[31−33] We present the full characterization of the nanoparticles, their photophysical properties which reveal unprecedented long iridium lifetimes in the cell and a variation of lifetime based on the environment. The results of nanoparticle localization in cells are also supported by total internal reflection fluorescence microscopy (TIRF), electron microscopy as well as inductively coupled plasma mass spectrometry (ICPMS) analysis.

RESULTS AND DISCUSSION

The iridium probe, IrC_6, was synthesized from the iridium dimer, $[Ir(ppy\text{-}C_6)_2(\mu\text{-}Cl)]_2$, and a surface active bipyridine ligand with long legs for attachment to gold (Scheme 2). The 2-(hexylphenyl)-pyridine ligand was synthesized based on the method of Ackermann et al.[34] and conjugated to iridium

Scheme 2. Synthetic Route for Preparation of IrC_6

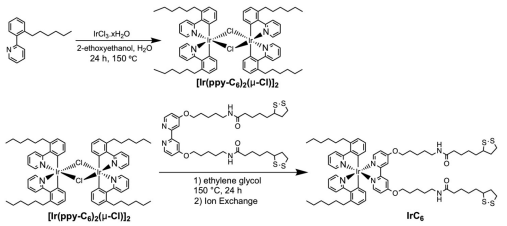

trichloride hydrate to form the iridium dimer $[Ir(ppy\text{-}C_6)_2(\mu\text{-}Cl)]_2$. The final step involved conjugation of the bipyridine ligand to the dimer to form IrC_6.[35] The iridium complex was fully characterized and its photophysical properties investigated.

The IrC_6 complex showed absorption bands in the UV−vis region (Figure S1 in the Supporting Information (SI)) with intense bands at 230 and 260 nm arising from the $^1\pi-\pi^*$ transitions from the ligands and a tail with shoulders at 300 and 350 nm, extending to 400 nm, which are attributed to ^{1}MLCT transitions in accordance with previous assignments.[36] Excitation of a solution of IrC_6 in water at 350 or 375 nm produced an emission broad peak with a maximum at 580 nm (Figure 1) which is attributed to a triplet charge transfer state

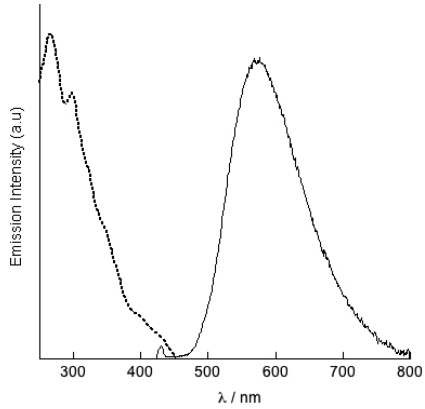

Figure 1. Photophysical characterization of IrC_6 in water. Excitation spectrum (dotted line) λ_{em} = 580 nm and luminescence spectra (solid line) of 30 μM Ir(C_6) in water λ_{exc} = 375 nm. Spectra are corrected for PMT and instrument response.

which usually has contributions of ^{3}MLCT and ^{3}LMCT.[37] The excitation spectrum showed the characteristic absorption profile, revealing that excitation in the range up to 430 nm is possible to provide emission which makes this complex a suitable candidate for conventional confocal microscopes. Upon addition of Zonyl FSA (10 μL 10% in water) to a solution of IrC_6 in water (30 μL) a 10 nm bathochromic shift was observed in emission (Figure S2 in the SI). The shift is indicative of an interaction of the probe with the surfactant, changing the environment around the IrC_6 probe and affecting the charge transfer transition. The quantum yield of a solution of IrC_6 was found to be 4% and the luminescence lifetime was analyzed with three components to be 42 ns (a_1 = 6%) 166 ns (a_2 = 45%), 428 ns (a_3 = 49%). These data agree with phenylpyridine iridium complexes previously studied.[36,38,39] Upon addition of Zonyl surfactant to a solution of IrC_6 a reduction of the lifetime is observed, notably a 160 ns decrease of the long-lived component [49 ns (a_1 = 3%), 147 ns (a_2 = 35%), 324 ns

DOI: 10.1021/jacs.8b05105
J. Am. Chem. Soc. 2018, 140, 10242−10249

(a_3 = 62%)] (Table S1 in the SI). This differs from the effect of the surfactant on a ruthenium complex, where a 25% lifetime enhancement was seen upon addition of the Zonyl surfactant.[22] This could be due to the effect of the hexyl chain and the lower charge of the complex in the interaction with the surfactant.

Monodisperse, water-soluble 13, 25, and 100 nm gold nanoparticles (AuNP13, AuNP25, and AuNP100) were synthesized using the improved Turkevich method, with slight modifications.[40−42] The protocol involved synthesizing AuNP13 seeds by a citrate reduction method, followed by a growth procedure to give AuNP25 and AuNP100 nanoparticles stabilized with citrate anions. These AuNPs were characterized by surface plasmon resonance (SPR), dynamic light scattering (DLS), zeta potential, and transmission electron microscopy (TEM).

AuNP13, AuNP25, and AuNP100 showed a characteristic SPR band with a maximum, λ_{max} (H_2O) at 517, 519, and 556 nm, respectively. AuNP13, AuNP25, and AuNP100 were sized by DLS analysis. The number distribution indicated sizes at 13 ± 3 nm (PDI = 0.07), 18 ± 5 nm (PDI = 0.05) and 80 ± 20 nm (PDI = 0.03), respectively (Table S2 in the SI). TEM images showed sizes of 15, 25, and 95 nm for AuNP13, AuNP25, and AuNP100 respectively, which agree with the DLS results (Figure S3 in the SI). Prior to coating with the IrC_6 complex, a fluorinated surfactant, Zonyl FSA was used to stabilize the nanoparticle surface and prevent aggregation induced by positively charged metals by direct replacement of the negative citrate ions. The surfactant-modified nanoparticles were isolated by centrifugation to give Z·AuNP13, Z·AuNP25, and Z·AuNP100. The IrC_6 complex is then added to the colloid. A solution of IrC_6 in MeOH (1 mM) was titrated in 2.5 μL aliquots to an aqueous solution of the corresponding Zonyl-coated nanoparticles and the SPR shift was monitored within the visible region (Figure 2). The observed red shift in

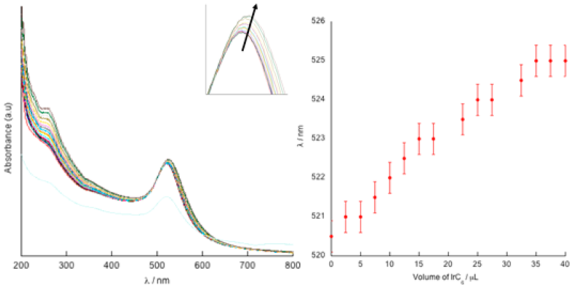

Figure 2. UV/vis titration of 1 mM IrC_6 into 1.6 nM Z·AuNP25 in water (left) and λ_{max} of SPR peak vs volume of IrC_6 (20 μM) added (right).

the SPR band confirmed the modification of the gold surfaces and allowed us to identify the saturation point of the maximum concentration of the iridium probe before aggregation of the particle. Addition of 20 μL, 40 and 30 μL of 1 mM IrC_6 into Z·AuNP13, Z·AuNP25, and Z·AuNP100 resulted in shifts of 5 (λ_{max} = 522 nm), 6 (λ_{max} = 525 nm), and 2 (λ_{max} = 558 nm) nm, respectively. The iridium-coated nanoparticles were isolated by size exclusion chromatography (Sephadex G10) to remove any excess molecular probe and produced IrC_6·AuNP13, IrC_6·AuNP25 and IrC_6·AuNP100. Following chromatography for isolation of these nanoparticles, the λ_{max} of the SPR band remained unchanged, showing that the surface coating has not been altered by the removal of the excess metal complex (Figure S4 in the SI).

DLS analysis of the iridium-coated nanoparticles showed that the size of the AuNPs did not significantly change when coated with Zonyl and IrC_6 (Table 1). Analysis of TEM images

Table 1. Dynamic Light Scattering Data for IrC_6·AuNP in Water, Showing Polydispersity Index (PDI) and Sizes by Number and Intensity Distributions

	PDI	size by number/nm	size by intensity/nm
IrC_6·AuNP13	0.27	17 ± 4	28 ± 10
IrC_6·AuNP25	0.18	22 ± 6	40 ± 18
IrC_6·AuNP100	0.02	90 ± 22	110 ± 25

showed spherical particles with estimated diameters of 15, 25, and 95 nm for IrC_6·AuNP13, IrC_6·AuNP25, and IrC_6·AuNP100, respectively (Figure 3). Elemental composition of

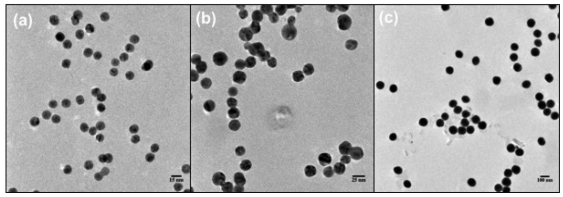

Figure 3. Transmission electron microscope images of (a) IrC_6·AuNP13, (b) IrC_6·AuNP25, and (c) IrC_6·AuNP100. Images were acquired on JOEL 1200 EX transmission electron microscopy. Scale bars are 15, 25, and 100 nm.

the nanoparticles by ICPMS showed a coating of 1400, 3200, and 22 000 IrC_6 complexes per AuNP for IrC_6·AuNP13, IrC_6·AuNP25, and IrC_6·AuNP100, respectively.

The photophysical properties of these functionalized nanoparticles were investigated by steady state and time-resolved spectroscopy to identify any changes in behavior of the IrC_6 complex when conjugated to the surface of the gold nanoparticle. All three different sized gold nanoparticles, IrC_6·AuNP13, IrC_6·AuNP25, and IrC_6·AuNP100 were emissive upon excitation at either 350, 375, or 405 nm, with a λ_{max} at 590 nm. The emission maximum was red-shifted by 10 nm in comparison to the free complex in water, which showed an emission λ_{max} at 580 nm, the shift being the same as in the presence of surfactant, reflecting the environment around the iridium probe. The luminescence spectrum of IrC_6·AuNP25 is shown in Figure 4 and the spectra for the rest of the nanoparticles can be found in the Supporting Information (Figure S5 in th SI).

The excitation spectra displayed the iridium characteristic bands and the shoulders around 400 and 420 nm which are responsible for the observed emission. The luminescence lifetime of IrC_6·AuNP25 in water was analyzed with three components to be 40 ns (a_1 = 5%), 160 ns (a_2 = 42%), and 330 ns (a_3 = 53%). Similar lifetimes were found for IrC_6 ·AuNP13 and IrC_6 ·AuNP100 respectively (Table S3, SI). Interestingly, the luminescence lifetimes of the iridium-coated gold nanoparticles reflect the reduction of the signal observed by the influence of the Zonyl surfactant environment rather than any quenching from the gold nanoparticle. The influence of the Zonyl surfactant is also evident in the observed shift of the λ_{max} in the emission spectrum of the nanoparticles in comparison with the IrC_6 molecular probe. The quantum

DOI: 10.1021/jacs.8b05105
J. Am. Chem. Soc. 2018, 140, 10242−10249

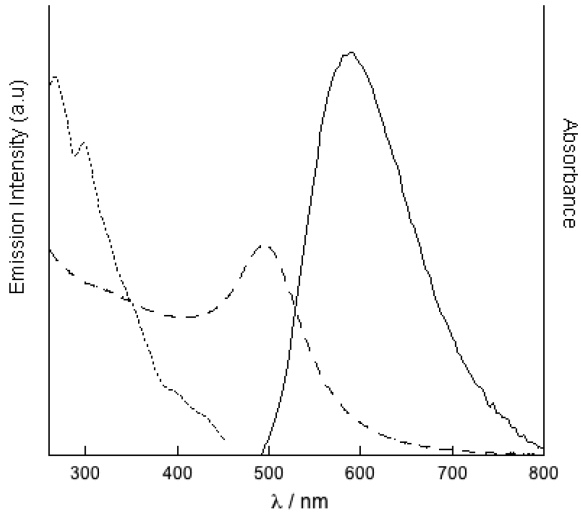

Figure 4. Steady-state emission λ_{exc} = 375 nm (solid line), UV/vis absorption (dashed line), and excitation, λ_{em} = 590 nm (dotted line) spectra of 1.6 nM IrC_6·AuNP25. Spectra are corrected for PMT and instrument response.

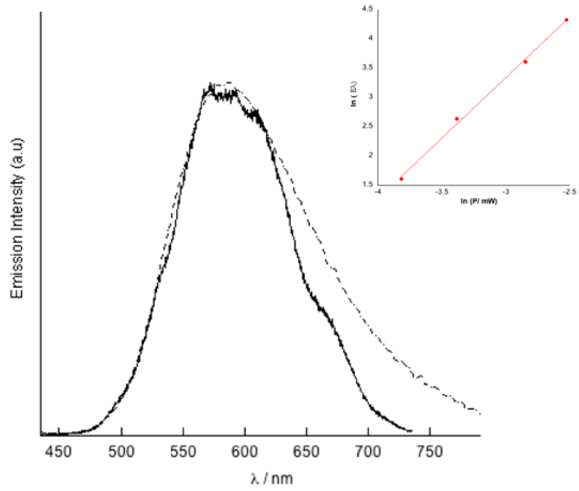

Figure 5. Emission spectra produced from one photon excitation λ_{exc} = 375 nm (dotted line) and two-photon excitation λ_{exc} = 760 nm (solid line) of IrC_6·AuNP25 in agarose gel. Spectra have been normalized. Inset: Power dependence study showing integrated intensity as a function of laser power for IrC_6 ·AuNP25 in agarose gel, gradient is 2.068 (R = 0.997). λ_{exc} = 760 nm.

yields of the IrC_6·AuNP13 and IrC_6·AuNP25 nanoparticles were found to be 5%, using an integrated sphere and the Zonyl coated gold nanoparticles as reference sample with an SPR to match the SPR peak of IrC_6-coated nanoparticles (Figure S6, SI). Determination of number of AuNPs per cell was carried out by ICPMS. It was found that there were approximately 67 000, 26 000, and 5100 AuNPs per cell for IrC_6·AuNP13, IrC_6·AuNP25, and IrC_6·AuNP100, respectively (SI). Further ICPMS analysis of mitochondria and vesicles isolated by cell fractionation show comparable accumulation in both mitochondria and vesicles which is increased by incubation time (from 6 to 24 h, Figure S16)

To examine the suitability of the nanoparticles for two photon imaging, we investigated the two-photon absorption cross sections and the power dependence analysis of their luminescence. The colloidal solution of IrC_6·AuNP25 was immobilized in 0.1% agarose gel to restrict the particle movement through the laser beam at a fast rate due to the Brownian motion. The laser dependence studies were calculated on four different areas of the agarose gel and the average was calculated. Two-photon excitation at 760 nm produced the same emission as one-photon excitation (Figure 5). The integrated emission intensity was plotted against the laser intensity showing a linear fit in a log−log plot. The slope of the linear fit was calculated to be 2, demonstrating the two-photon process which is taking place. The two-photon absorption cross sections ($\sigma 2$) were calculated for both the IrC_6 probe in methanol and IrC_6·AuNP25 in 0.1% agarose gel using the equation below, which compares the luminescence intensity of the samples to that of a reference standard, rhodamine B in methanol.[43]

$$\sigma_{2s} = \frac{C_r}{C_s}\frac{I_{\lambda s}}{I_{\lambda r}}\frac{(FI_{\lambda r}/(\sum FI_r))}{(FI_{\lambda s}/(\sum FI_s))}\frac{\phi_r}{\phi_s}\sigma_{2r}$$

where r and s stand for the reference standard and sample respectively, $\sigma 2$ for two-photon absorption cross section, c for concentration, FI_λ and FI_λ are the fluorescence intensity at the wavelength λ for two-photon and one-photon, respectively. ΣFL describes the integrated intensity of the one-photon fluorescence spectra, and ϕ is the one-photon fluorescence quantum yield, which is assumed to be the same under two-photon conditions.[44] The results showed an absorption cross section of 38 GM (GM = 10^{-50} cm^4 s $photon^{-1}$) for the IrC_6 in methanol and 2 × 10^3 GM of IrC_6·AuNP25. The absorption cross section calculated for IrC_6 agrees with similar iridium compounds.[45] The absorption cross section of IrC_6·AuNP25, is unprecedently high for any iridium-based luminescence signal and is attributed to the enhancement by the gold surface plasmon resonance.

Two-photon lifetime imaging of live HeLa cells treated with iridium nanoparticles was employed to monitor long and short lifetimes in two different channels for nanoparticle localization. The lifetime-based detection of the HeLa cells in these two channels is shown in Figure 6 for IrC_6·AuNP25, IrC_6·AuNP100, and IrC_6·AuNP13. One channel was set to detect the long component of the iridium signal in the hundreds of nanoseconds range and the second channel was set to detect a short-lived signal in the tens of picosecond range which became apparent that this originated from the gold nanoparticle surface plasmon resonance, supported by the lifetime decay (Figure S7, SI). These short-lived picosecond lifetimes, in the range of 20−120 ps, were detected in HeLa cells showing uptake of IrC_6 ·AuNPs, this can be seen in yellow in Figure 6. The detection in the nanosecond range reveal lifetimes which were longer than the iridium nanoparticles in solution. We analyzed these images to find lifetimes in the range of 450−1000 ns, which can be seen in red in Figure 6. The lifetimes displayed in the long-lived channel are the long component (τ_3). The three sizes of nanoparticles show a similar pattern, with uptake dominated in the cytoplasm of the cell and some presence in the nucleus. which is more dominant for IrC_6·AuNP25 and IrC_6·AuNP13. The uptake of IrC_6·AuNP100 differs from that of IrC_6·AuNP13 and IrC_6·AuNP25 with more clusters of nanoparticles being formed around the outer cell membrane, clearly evidenced by the gold signal. The clustering could be due to the larger size of nanoparticles slowing down uptake and confining these nanoparticles to the cellular membrane, slowing down uptake due to steric hindrance and receptor saturation.[33] Stacks of the images

DOI: 10.1021/jacs.8b05105
J. Am. Chem. Soc. 2018, 140, 10242−10249

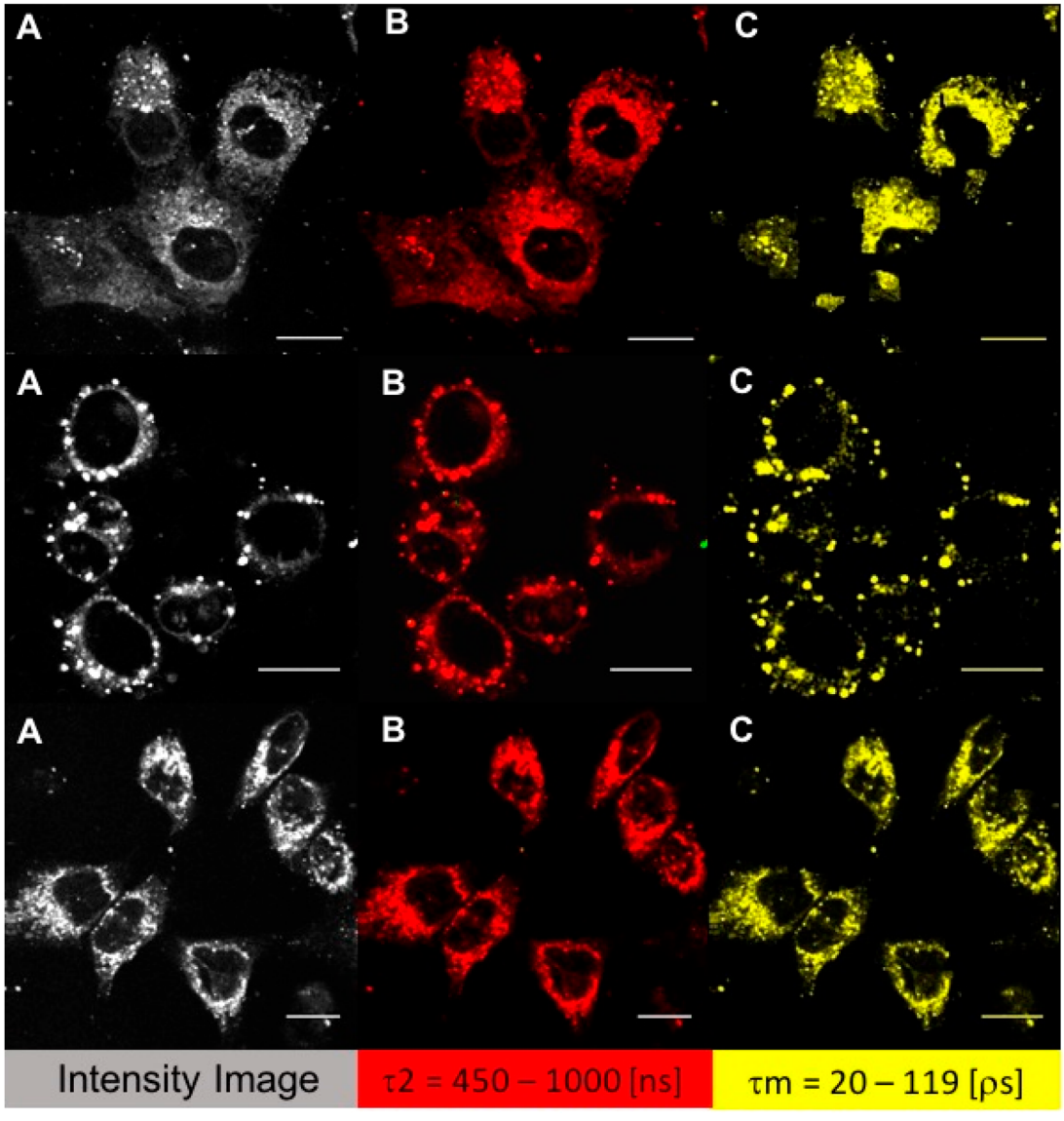

Figure 6. Two photon, two channel lifetime microscopy of IrC_6·AuNP25 (top), IrC_6·AuNP100 (middle), and IrC_6·AuNP13 (bottom) in live HeLa cells. (A) Intensity image. (B) Image of iridium signal showing a lifetime range of 450−1000 ns (red). (C) Image of short-lived signal showing a lifetime range of 20−120 ps, from the gold. HeLa cells incubated with 0.16 nM IrC_6·AuNP25 for 3 h and 0.45 nM IrC_6·AuNP13 and 3 pM IrC_6·AuNP100 for 5 h. λ_{exc} = 760 nm, scale bar = 20 μm.

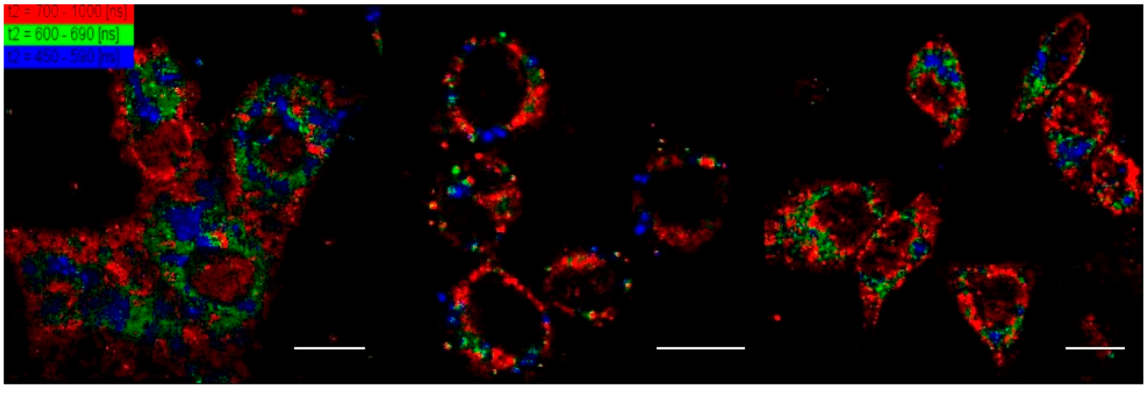

Figure 7. Mapping the iridium signal of iridium-coated nanoparticles in live HeLa cells: IrC_6·AuNP25 (left), IrC_6·AuNP100 (middle), and IrC_6·AuNP13 (right). Image of signal with a lifetime range of 700−1000 ns (red), 600−690 ns (green), and 450−590 ns (blue). HeLa cells incubated with 0.16 nM IrC_6·AuNP25 for 3 h and 0.45 nM IrC_6·AuNP13 and 3 pM IrC_6·AuNP100 for 5 h. λ_{exc} = 760 nm, scale bar = 20 μm.

DOI: 10.1021/jacs.8b05105
J. Am. Chem. Soc. 2018, 140, 10242−10249

throughout the cell show the nanoparticle localization (SI, Figure S17).

We investigated the lifetime variation within the cell. We identified three areas to map the variation of the τ_2 of the iridium nanoparticle signal in the cell: cytoplasm, nucleus and nanoparticle clusters (Figure 7). The lifetime variation was mapped by taking the average of at least 10 lifetimes of the different areas. It was found that the iridium lifetime in the cytoplasm extends to 665, 650, and 660 ns with a standard deviation of ±75 ns. This range was evident for all the nanoparticles, IrC_6·AuNP13, IrC_6·AuNP25, and IrC_6·AuNP100. These average lifetimes observed for the iridium long component show an increase of 320 ± 10 ns from the iridium-coated gold nanoparticles recorded in water. The largest increase seen is within the nucleus of the cell, in some other areas of the cell (colored in red) where the average lifetimes observed are 740 ± 80 ns (Figure 7). These lifetimes are higher by 400 ns from the iridium-coated gold nanoparticles recorded in water. Evidence of nuclear localization of some of the nanoparticles is further supported by confocal luminescence imaging using Hoechst nuclear stain and recording z-stacks of the iridium and Hoechst signals (SI, Figures S14 and S15). The presence of the long-lived signal in the nucleus is much weaker for the IrC_6 ·AuNP100 with their localization confined to the cell membrane and cytoplasm but it is sensitive to be detected for the smaller nanoparticles (Figure S8, SI) whose localization in the nucleus can be more challenging to be detected with other microscopy techniques which require high concentrations and accumulations of particles. It was clear that clusters of nanoparticles seem to be accompanied by lifetimes highlighted in 450−590 ns (colored blue). The lifetime variation at this range shows more clusters present in the IrC_6 ·AuNP25 than for the IrC_6·AuNP13.

To further understand the effect of the change in lifetime of these nanoparticles, the lifetimes of the iridium-functionalized nanoparticles were recorded in full cell media (DMEM with 10% fetal bovine serum, FBS, 5% penicillin−streptomycin−glutamine) and FBS (90% v/v) to emulate the conditions in a cell (Table 2). It is clearly observed that the iridium nanoparticles showed a large increase in lifetime when measured in cell media and FBS serum with the IrC_6·AuNP25 showing the largest increase of 145 and 265 ns when measured in cell media and FBS respectively. The SPR of IrC_6·AuNP25 was checked by UV/vis to prove no aggregation was occurring when placed in cell media (Figure S9, SI). We postulate that the long lifetimes of the iridium nanoparticles in cells reflect their interaction with cellular chemicals and proteins. The lifetime of the molecular complex IrC_6 is also affected by cell media and FBS although the increase is not as enhanced as seen on the nanoparticles.

Table 2. Lifetimes Recorded for Samples in Water, Cell Media, and FBS Serum[a]

	lifetimes under different conditions (ns)		
	IrC_6·AuNP13	IrC_6·AuNP25	IrC_6 ·AuNP100
water	50 (5%)	40 (5%)	25 (3%)
	180 (48%)	160 (42%)	140 (43%)
	340 (47%)	330 (53%)	340 (54%)
cell media	13 (5%)	16 (2%)	30 (2%)
	120 (15%)	125 (12%)	160 (22%)
	450 (80%)	475 (86%)	440 (76%)
FBS serum	14 (5%)	21 (3%)	10 (5%)
	121 (17%)	161 (13%)	110 (20%)
	515 (78%)	565 (84%)	530 (85%)

[a]Lifetimes were recorded using a 376 nm laser and were fitted with a χ^2 between 1 and 1.1.

To assess nanoparticle clustering in the cells, we examined the average lifetime of these clusters in the cells for the different sized nanoparticles and compared them with nanoparticles in solution, forced into aggregation by addition of 50 mM Tris buffer (Figure S10, SI). The lifetimes of aggregated particles in solution showed an increase in the contribution of the shorter component to 170 ns (63%), in comparison to 160 ns (42%) for IrC_6·AuNP25 in water and a decrease in the long component to 300 ns (33%), in comparison to 330 ns (53%) for IrC_6·AuNP25 in water. These values are much shorter than the main component observed in cells, for all three sizes of nanoparticles, which is over 450 ns. The data confirm that the observed clusters are indeed nonaggregated nanoparticles. It is therefore concluded that the nanoparticles have come together during uptake to form clusters within the cell rather than aggregated particles. Notably, the iridium lifetime within the cells is clearly longer than that observed of the nanoparticles in solution. The lifetimes of the IrC_6 probe and the nanoparticles in water are shown for comparison.

To further analyze the internalization of the IrC_6·AuNP25, we used TIRF microscopy. TIRF provides high-resolution imaging of the cell surface,[46,47] which allowed us to determine localization of these nanoparticles throughout the cell (Figure 8) as TIRF angle is varied. Clear bright white spots in the luminescence image (planes 1−5) are attributed to iridium luminescence from the nonclustered gold nanoparticles on planes moving upward from the imaging dish. This shows nanoparticle localization within the cell more specifically in the cytoplasm and around the cell membrane, which agrees with the lifetime imaging studies. Most importantly, the images show clearly nonaggregated nanoparticles with good resolution. TIRF microscopy is governed by the evanescent wave with the resolution restricted to 150 nm depth, providing information inside the cell membrane. TIRF clearly shows nonclustered, single nanoparticles in each plane.

Transmission electron microscopy images showed the IrC_6·AuNP25 nanoparticles to appear as dark spheres located throughout the cytoplasm of the cell (Figure S11). They appeared to be individual spheres with the predicted size of individual particles, suggesting that no aggregation occurs upon uptake. The nanoparticles are localized within vesicles suggesting the mechanism of uptake could be endocytosis.[33] These vesicles contain a high number of nanoparticles which have been taken up together. Since these nanoparticles have localized in one place, at lower magnifications they may appear to have formed "clusters" within the cell. The ICPMS results also support the presence of nanoparticles in vesicles (SI, Figure S16). The IrC_6·AuNP100 showed localization around the outer and inner cell membrane supporting the two-photon lifetime imaging studies.

CONCLUSIONS

We have shown that surface-active iridium complexes attached to gold nanoparticles of different sizes show characteristically long luminescence lifetimes and emission in the visible range. The fluorinated surfactant used to stabilize gold nanoparticles

DOI: 10.1021/jacs.8b05105
J. Am. Chem. Soc. 2018, 140, 10242−10249

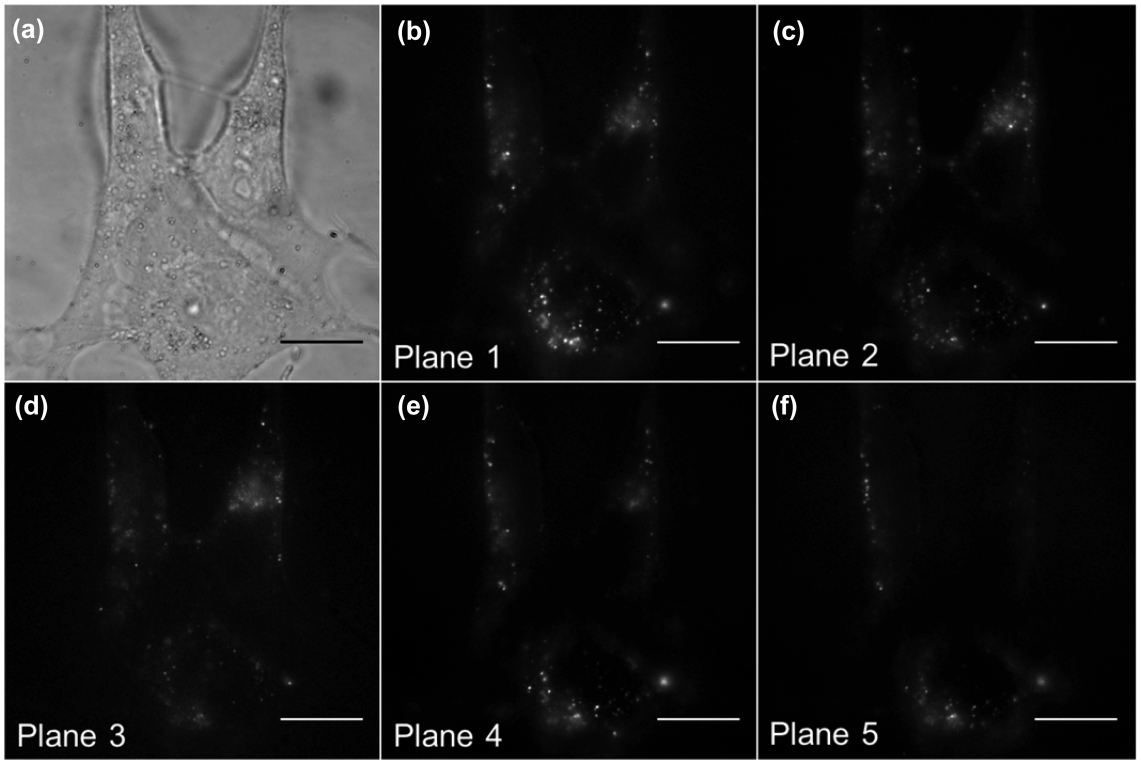

Figure 8. Total internal reflectance fluorescence microscopy (TIRF) of 0.16 nM IrC_6·AuNP25 in HeLa cells after incubation of 3 h. (a) Bright field and (b–f) TIRF images demonstrating internalization of gold nanoparticles. λ_{exc} = 405 nm.

led to reduction in the lifetime of the iridium complex in solution; however, no further decrease was detected upon attachment to the different sized nanoparticles. The iridium-coated nanoparticles displayed two-photon luminescence in agreement with the one-photon spectra and a two-photon absorption cross section much higher than the molecular probe attributed to the gold nanoparticle. Two-photon lifetime imaging of the iridium-coated nanoparticles in cancer cells demonstrated that detection can be performed in two channels, one for the long lifetime signal of the iridium complex in hundreds of nanoseconds and the other for the short lifetime signal from the gold in tens of picoseconds. The two-channel detection showed clearly the iridium and gold signal for all nanoparticle sizes investigated, with uptake being seen in the cytoplasm and nucleus of the cells. It was found that the majority of 100 nm AuNPs located around the cell plasma membrane. Remarkably long lifetimes have been detected in the cell, with the nanoparticles localized in the nucleus showing an average of 740 ns. Clusters of the nanoparticles showed lifetimes of 450–590 ns and are found in the cytoplasm but not in the nucleus of the cells. The IrC_6·AuNP25 showed more clustering than the IrC_6·AuNP13. The clustering of the nanoparticles was also supported by TEM images, although nanoparticles in the nucleus were not detected, possibly due to the small sections of cell slices. Nuclear localization of small nonaggregated nanoparticles is challenging but the sensitivity of the luminescence lifetime signal demonstrated nuclear localization by detecting the long-lived lifetimes, which was more dominant for the IrC_6·AuNP13 and IrC_6·AuNP25. We have independently examined the nanoparticle lifetime variation in solution upon addition of serum, and it is apparent that lengthening of the lifetimes is observed which is attributed to interactions of the nanoparticles with biomolecules. Clustering of nanoparticles showed shorter lifetimes but not as short as aggregated particles, confirming that these clusters were in fact non-aggregated particles. Overall, the iridium-coated nanoparticles are introduced as novel nanoprobes for two-photon lifetime imaging with unprecedented long lifetimes, providing multi-channel detection for independent monitoring of the gold scaffold and the iridium signal. The long-lived lifetime signal is sensitive to the cell environment, providing local information which can be used for gating specific biomolecular interactions and tracking nanoparticles in in vivo models.

■ ASSOCIATED CONTENT

Supporting Information

The Supporting Information is available free of charge on the ACS Publications website at DOI: 10.1021/jacs.8b05105.

UV–vis spectra of IrC_6 and nanoparticles, DLS results, TEM of nanoparticles, luminescence lifetime analysis of images, confocal fluorescence microscopy images, Z-stack, 3D stack of lifetime images and video shots (PDF)

Z-Stack of short-lived picosecond lifetimes from the gold in live HeLa cells dosed with 0.16 nM IrC_6·AuNP25 for 24 hours (AVI)

Z-Stack of long-lived nanosecond lifetimes in live HeLa cells dosed with 0.16 nM IrC_6·AuNP25 for 24 hours (AVI)

■ AUTHOR INFORMATION

Corresponding Author

*z.pikramenou@bham.ac.uk

ORCID

Zoe Pikramenou: 0000-0002-6001-1380

DOI: 10.1021/jacs.8b05105
J. Am. Chem. Soc. 2018, 140, 10242–10249

Notes

The authors declare no competing financial interest.

■ ACKNOWLEDGMENTS

We wish to thank EPSRC-Doctoral Training Centre for support (EP/F50053X/1) and the Leverhulme Trust and the University of Birmingham for financial support. R.I.T. thanks the Brazilian National Council for Scientific and Technological Development (CNPq-SWG/215833/2013-9) for funding.

■ REFERENCES

(1) Brown, E. B.; Campbell, R. B.; Tsuzuki, Y.; Xu, L.; Carmeliet, P.; Fukumura, D.; Jain, R. K. *Nat. Med.* **2001**, *7*, 1069.
(2) McDonald, D. M.; Choyke, P. L. *Nat. Med.* **2003**, *9*, 713.
(3) Zipfel, W. R.; Williams, R. M.; Webb, W. W. *Nat. Biotechnol.* **2003**, *21*, 1369.
(4) Bunzli, J. C. G. *Chem. Rev.* **2010**, *110*, 2729.
(5) Berezin, M. Y.; Achilefu, S. *Chem. Rev.* **2010**, *110*, 2641.
(6) Sperling, R. A.; Rivera gil, P.; Zhang, F.; Zanella, M.; Parak, W. J. *Chem. Soc. Rev.* **2008**, *37*, 1896.
(7) Dreaden, E. C.; Alkilany, A. M.; Huang, X. H.; Murphy, C. J.; El-Sayed, M. A. *Chem. Soc. Rev.* **2012**, *41*, 2740.
(8) Cheng, X. Y.; Hinde, E.; Owen, D. M.; Lowe, S. B.; Reece, P. J.; Gaus, K.; Gooding, J. J. *Adv. Mater.* **2015**, *27*, 6144.
(9) Zhang, J.; Fu, Y.; Conroy, C. V.; Tang, Z. H.; Li, G.; Zhao, R. Y.; Wang, G. L. *J. Phys. Chem. C* **2012**, *116*, 26561.
(10) Teixeira, R.; Serra, V. V.; Paulo, P. M. R.; Andrade, S. M.; Costa, S. M. B. *RSC Adv.* **2015**, *5*, 79050.
(11) Boreham, A.; Brodwolf, R.; Walker, K.; Haag, R.; Alexiev, U. *Molecules* **2017**, *22*, 17.
(12) Lemon, C. M.; Karnas, E.; Han, X. X.; Bruns, O. T.; Kempa, T. J.; Fukumura, D.; Bawendi, M. G.; Jain, R. K.; Duda, D. G.; Nocera, D. G. *J. Am. Chem. Soc.* **2015**, *137*, 9832.
(13) Byrne, A.; Burke, C. S.; Keyes, T. E. *Chem. Sci.* **2016**, *7*, 6551.
(14) Lo, K. K. *Acc. Chem. Res.* **2015**, *48*, 2985.
(15) Fernandez-Moreira, V.; Thorp-Greenwood, F. L.; Coogan, M. P. *Chem. Commun.* **2010**, *46*, 186.
(16) Henwood, A. F.; Zysman-Colman, E. *Chem. Commun.* **2017**, *53*, 807.
(17) Venkatesh, V.; Berrocal-Martin, R.; Wedge, C. J.; Romero-Canelon, I.; Sanchez-Cano, C.; Song, J. I.; Coverdale, J. P. C.; Zhang, P. Y.; Clarkson, G. J.; Habtemariam, A.; Magennis, S. W.; Deeth, R. J.; Sadler, P. J. *Chem. Sci.* **2017**, *8*, 8271.
(18) Botchway, S. W.; Charnley, M.; Haycock, J. W.; Parker, A. W.; Rochester, D. L.; Weinstein, J. A.; Williams, J. A. G. *Proc. Natl. Acad. Sci. U. S. A.* **2008**, *105*, 16071.
(19) Zheng, X.; Tang, H.; Xie, C.; Zhang, J.; Wu, W.; Jiang, X. *Angew. Chem., Int. Ed.* **2015**, *54*, 8094.
(20) Zhang, S. J.; Hosaka, M.; Yoshihara, T.; Negishi, K.; Iida, Y.; Tobita, S.; Takeuchi, T. *Cancer Res.* **2010**, *70*, 4490.
(21) Rogers, N. J.; Jeffery, H. C.; Claire, S.; Lewis, D. J.; Zikeli, G.; Hodges, N. J.; Egginton, S.; Nash, G. B.; Pikramenou, Z. *Nanomedicine* **2017**, *12*, 2725.
(22) Osborne, S. A. M.; Pikramenou, Z. *Faraday Discuss.* **2015**, *185*, 219.
(23) Maldonado, C. R.; Salassa, L.; Gomez-Blanco, N.; Mareque-Rivas, J. C. *Coord. Chem. Rev.* **2013**, *257*, 2668.
(24) Boisselier, E.; Astruc, D. *Chem. Soc. Rev.* **2009**, *38*, 1759.
(25) Rogers, N. J.; Claire, S.; Harris, R. M.; Farabi, S.; Zikeli, G.; Styles, I. B.; Hodges, N. J.; Pikramenou, Z. *Chem. Commun.* **2014**, *50*, 617.
(26) Davies, A.; Lewis, D. J.; Watson, S. P.; Thomas, S. G.; Pikramenou, Z. *Proc. Natl. Acad. Sci. U. S. A.* **2012**, *109*, 1862.
(27) Varnavski, O. P.; Mohamed, M. B.; El-Sayed, M. A.; Goodson, T. *J. Phys. Chem. B* **2003**, *107*, 3101.
(28) Shang, L.; Azadfar, N.; Stockmar, F.; Send, W.; Trouillet, V.; Bruns, M.; Gerthsen, D.; Nienhaus, G. U. *Small* **2011**, *7*, 2614.
(29) Komatsu, H.; Yoshihara, K.; Yamada, H.; Kimura, Y.; Son, A.; Nishimoto, S.; Tanabe, K. *Chem. - Eur. J.* **2013**, *19*, 1971.
(30) Jiang, W. L.; Gao, Y.; Sun, Y.; Ding, F.; Xu, Y.; Bian, Z. Q.; Li, F. Y.; Bian, J.; Huang, C. H. *Inorg. Chem.* **2010**, *49*, 3252.
(31) Liu, X. S.; Huang, N.; Li, H.; Jin, Q.; Ji, J. *Langmuir* **2013**, *29*, 9138.
(32) Chithrani, B. D.; Ghazani, A. A.; Chan, W. C. W. *Nano Lett.* **2006**, *6*, 662.
(33) Hoshyar, N.; Gray, S.; Han, H. B.; Bao, G. *Nanomedicine* **2016**, *11*, 673.
(34) Ackermann, L.; Novak, P.; Vicente, R.; Hofmann, N. *Angew. Chem., Int. Ed.* **2009**, *48*, 6045.
(35) Adams, S. J.; Lewis, D. J.; Preece, J. A.; Pikramenou, Z. *ACS Appl. Mater. Interfaces* **2014**, *6*, 11598.
(36) Lamansky, S.; Djurovich, P.; Murphy, D.; Abdel-Razzaq, F.; Kwong, R.; Tsyba, I.; Bortz, M.; Mui, B.; Bau, R.; Thompson, M. E. *Inorg. Chem.* **2001**, *40*, 1704.
(37) Colombo, M. G.; Hauser, A.; Gudel, H. U. *Inorg. Chem.* **1993**, *32*, 3088.
(38) Lo, K. K. W.; Ng, D. C. M.; Chung, C. K. *Organometallics* **2001**, *20*, 4999.
(39) Lowry, M. S.; Bernhard, S. *Chem. - Eur. J.* **2006**, *12*, 7970.
(40) Schulz, F.; Homolka, T.; Bastus, N. G.; Puntes, V.; Weller, H.; Vossmeyer, T. *Langmuir* **2014**, *30*, 10779.
(41) Wuithschick, M.; Birnbaum, A.; Witte, S.; Sztucki, M.; Vainio, U.; Pinna, N.; Rademann, K.; Emmerling, F.; Kraehnert, R.; Polte, J. *ACS Nano* **2015**, *9*, 7052.
(42) Ziegler, C.; Eychmuller, A. *J. Phys. Chem. C* **2011**, *115*, 4502.
(43) Xu, C.; Webb, W. W. *J. Opt. Soc. Am. B* **1996**, *13*, 481.
(44) Mathai, S.; Bird, D. K.; Stylli, S. S.; Smith, T. A.; Ghiggino, K. P. *Photoch. Photobio. Sci.* **2007**, *6*, 1019.
(45) Edkins, R. M.; Bettington, S. L.; Goeta, A. E.; Beeby, A. *Dalton. Trans.* **2011**, *40*, 12765.
(46) Betzig, E.; Patterson, G. H.; Sougrat, R.; Lindwasser, O. W.; Olenych, S.; Bonifacino, J. S.; Davidson, M. W.; Lippincott-Schwartz, J.; Hess, H. F. *Science* **2006**, *313*, 1642.
(47) Mattheyses, A. L.; Simon, S. M.; Rappoport, J. Z. *J. Cell Sci.* **2010**, *123*, 3621.

DOI: 10.1021/jacs.8b05105
J. Am. Chem. Soc. 2018, 140, 10242−10249